Electron Spin Resonance Spectroscopy of Single Crystals of Concanavalin A

Eva Meirovitch, Zeev Luz,* and A. Joseph Kalb (Gilboa)

Contribution from the Isotope Department and the Department of Biophysics, The Weizmann Institute of Science, Rehovot, Israel. *Received March 7, 1974*

Abstract: An electron spin resonance (esr) study, at 35 GHz, of single crystals of Mn^{2+},Ca^{2+}-concanavalin A is reported. The Mn^{2+} spectrum is interpreted in terms of a spin hamiltonian with an isotropic g tensor, nearly isotropic hyperfine tensor, and a quadratic zero field splitting (ZFS) interaction. The $\pm 5/2 \leftrightarrow \pm 3/2$ and $\pm 3/2 \leftrightarrow \pm 1/2$ fine structure transitions are highly broadened by a large distribution in the ZFS parameters, making a quantitative interpretation of these lines impractical. The $1/2 \leftrightarrow -1/2$ transitions are relatively sharp and show sufficient second-order effects to allow a detailed study of the magnetic parameters of the Mn^{2+} ions. These are: $g_{Mn} = 2.0009$, $A_{\parallel} = 94.4$ G, $A_{\perp} = 91.5$ G, $D = 232$ G, and $\lambda = E/D = 0.185$. The distribution in the ZFS parameters is estimated to be ≤ 80 G and $\leq 5°$ in the magnitude and direction of its major component. It is suggested that this spread reflects a distribution in the local ligand structure of the metal binding site.

Concanavalin A is a saccharide-binding protein of the Jack bean.[1] In its native state, the protein contains manganese and calcium. Direct binding studies of the protein in solution have defined two distinct metal-binding sites: a transition metal-binding site, S1, and a calcium-binding site, S2. Both sites must be occupied for saccharide binding to occur.[2,3] Crystals of Mn^{2+},Ca^{2+}-concanavalin A belong to the orthorhombic space group I_{222} and are composed of identical subunits of molecular weight 26,000 daltons,[4] tetrahedrally arranged in clusters of four[5] (see Figure 1). The unit cell parameters are $a = 87.2$ Å, $b = 89.2$ Å, and $c = 62.9$ Å. X-Ray diffraction studies of the three-dimensional structure of concanavalin A have been reported recently.[6-8]

In the present work, we have used electron spin resonance (esr) spectroscopy to study the spin hamiltonian parameters of Mn^{2+} in single crystals of Mn^{2+},Ca^{2+}-concanavalin A. Relatively little work has been done on the esr of Mn^{2+} in proteins and the few published studies were done on solutions only.[9-16] Because of the slow tumbling rate of the protein molecules, the solution spectra are powder-like and difficult to interpret.[16] Furthermore, solution spectra do not yield information on the orientation of anisotropic interactions with respect to the protein molecules. These limitations are removed for single crystals as is well demonstrated in the present work.

Experimental Section

Single crystals of Mn^{2+},Ca^{2+}-concanavalin A were grown as described previously.[6]

Esr measurements were performed on a Varian E-12 spectrometer at Q band (35 GHz) at room temperature in a TE_{011} cavity. Measurements were made in the three crystallographic planes (*ab*, *bc*, and *ca*) at intervals of ~10°. The field was calibrated relative to the signal of DPPH, for which $g_{DPPH} = 2.0037$ was taken. For optimal measurements we used crystals of about 1-mm length. Larger crystals caused a large dielectric loss of microwave power in the cavity, while smaller crystals were susceptible to fast drying out and also gave signals too weak for accurate measurements.

The crystals were manipulated under water and care was taken to keep them moist at all times. For the measurements, they were sealed in thin-walled quartz capillaries containing a tiny drop of water.

The crystals are elongated along the *a* axis and it is therefore easy, with the aid of a polarizing microscope, to mount them with the *a* axis nearly parallel to the capillary axis. The precise orientation was determined by X-ray diffraction techniques as follows. One tip of the capillary was glued to the bottom of a short brass cup which fitted snugly into a hole drilled along the axis of the esr cavity basepiece. The height of the capillary could be adjusted by sliding the brass cup up and down with the aid of a small steel rod which screwed into its lower end. This adjustment was necessary since the optimal height of the crystal above the cavity base was different in the X-ray and in the esr measurements. The entire assembly was mounted on the goniometric head of an X-ray precession camera for crystallographic measurements and final adjustments. Short exposure (<5 min) Laue and precession photographs (Cu Kα $\bar{\mu} = 3°$, unscreened) were used to determine the precise orientation of the crystals. Only crystals with the *a* axis vertical to within 1° relative to the cavity base were used for the esr measurements in the *bc* plane.

For measurements in the other planes, the crystal was sealed in an arbitrary orientation in a short capillary (<2 mm), which was glued to a wooden stick clamped to an X-ray goniometer head. The directions of the crystallographic axes were determined by X-ray photography as above. The capillary was then reoriented and transferred with the aid of a transfer goniometer to the base of the esr cavity, so that either the *b* or *c* axis was perpendicular to the cavity base. The accuracy of mounting in these directions was somewhat less than that for the *bc* plane.

The Spin Hamiltonian and Symmetry Considerations

Esr spectra of $Mn^{2+}(^6S)$ are well described by the following spin hamiltonian

$$\mathcal{H} = g_{Mn}\beta HS + ASI + D[S_z^2 - 1/3\,S(S+1)] + E(S_x^2 - S_y^2) \qquad (1)$$

where the g and A tensors are taken as isotropic and the coordinates x, y and z refer to the principal directions of the quadratic zero field splitting (ZFS) tensor. The anisotropy of the spectrum thus results from the ZFS terms D and E. These terms split the esr spectrum of Mn^{2+} into five fine structure components of relative intensities 5, 8, 9, 8, and 5 and each of these components is further split into six by the hyperfine interaction, A.

Before discussing the experimental results it is useful to introduce some symmetry considerations which will facilitate the interpretation of the single crystal spectra. Since the crystal belongs to the crystallographic space group I_{222}, there are eight symmetry-related Mn^{2+} ions per unit cell: two groups of four centered respectively at the origin and the center of the cell.[6] The four manganese ions in each group are related by the symmetry operations of the point group 222, and for the discussion of the esr results it is sufficient to consider the symmetry of this point group only.[17] A schematic representation of the four Mn^{2+} sites, reflecting this symmetry, is shown in Figure 1, where we have arbitrarily numbered the sites 1 to 4. It then follows that in a general orientation of the magnetic field, the Mn^{2+} ions are nonequivalent and the esr spectrum will consist of four distinct spectra. When the magnetic field is parallel to a crys-

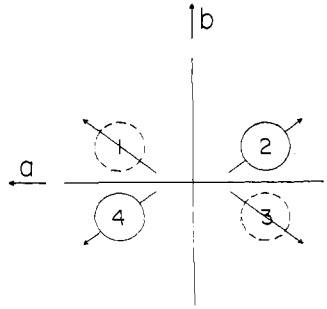

Figure 1. Schematic diagram of a tehahedral cluster of four asymmetric units related by 222 symmetry. Solid lines and dotted lines are above and below the *ab* plane, respectively. The Mn^{2+} ions are represented by circles and are arbitrarily numbered 1 to 4. The *c* axis is perpendicular to the plane of the figure.

tallographic plane the spectra will exactly coincide in pairs. Thus, when H is in the *ab* plane the equivalent pairs are (1, 3) and (2, 4), in the *ac* plane (1, 4) and (2, 3), and in the *bc* plane (1, 2) and (3, 4). Finally, when the magnetic field is along a crystallographic axis, all four Mn^{2+} sites are magnetically equivalent and their spectra will coincide exactly. It is therefore convenient to preform the esr experiments with the magnetic field parallel to the crystallographic planes, since then at most two spectra are observed.

For the interpretation of the spectra we are also interested in the connection between the Euler angles characterizing the principal coordinate axes of the ZFS tensor in the various sites. If we designate by α, β, γ the angles that transform the crystallographic axes *c*, *b*, *a* to the principal coordinate axes *x*, *y*, *z* of the ZFS tensor of site 1, then 222 symmetry implies that the corresponding angles for the other sites are as shown in Table I.[18] It should be emphasized that it is not possible to associate a given experimental spectrum with a particular asymmetric unit. There will, therefore, remain a fourfold ambiguity in determining the principal directions of the ZFS tensor relative to a given protein subunit.

Table I. Relation between the Euler Angles of the Four Symmetry Related Sites of Figure 1

Site 1	α	β	γ
Site 2	$180 + \alpha$	β	γ
Site 3	$-\alpha$	$180 - \beta$	$180 + \gamma$
Site 4	$180 - \alpha$	$180 - \beta$	$180 + \gamma$

Results and Interpretation

(i) First-Order Anisotropy of the Spectrum. Preliminary studies of the spectrum showed that the ZFS interaction is small compared to the Zeeman interaction. In this case the resonance field $H(M,m)$ (at constant microwave frequency, ν) of the various "allowed" hyperfine transitions ($M,m \leftrightarrow M-1,m$) is given to first order by[19]

$$H(M,m) = H_0 - (M - \tfrac{1}{2})\left[\frac{D}{g_{Mn}\beta}(3\cos^2\theta - 1) - \frac{E}{g_{Mn}\beta}3(\cos^2\theta - 1)\cos 2\phi\right] - \frac{A}{g_{Mn}\beta}m \quad (2)$$

where M and m are the electronic and nuclear azimuthal components of the spin angular momentum, $H_0 = h\nu/g_{Mn}\beta$, and θ and ϕ are the polar and azimuthal angles of the magnetic field direction in the principal coordinate system of the ZFS tensor. In this approximation the $\frac{1}{2},m \leftrightarrow -\frac{1}{2},m$ transitions are invariant with respect to rotation of the magnetic field, but the $\pm\frac{5}{2} \leftrightarrow \pm\frac{3}{2}$ and $\pm\frac{3}{2} \leftrightarrow \pm\frac{1}{2}$ are highly anisotropic.

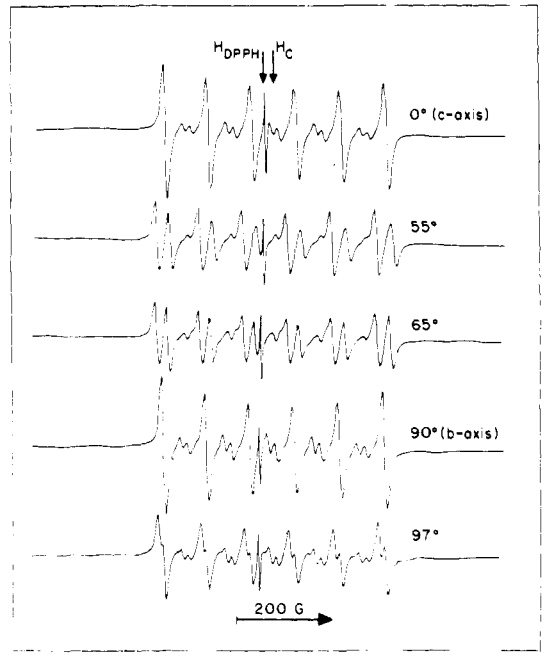

Figure 2. Q band esr spectra of a single crystal of Mn^{2+},Ca^{2+}-concanavalin A with the magnetic field in the *bc* plane. The angles indicate the orientation of the magnetic field with respect to the *b* axis. The sharp peaks are $\frac{1}{2} \leftrightarrow -\frac{1}{2}$ fine structure transitions, while the weak, broad bands on each side are $|\frac{5}{2}| \leftrightarrow |\frac{3}{2}|$ and $|\frac{3}{2}| \leftrightarrow |\frac{1}{2}|$ transitions. The arrow for H_C at the top refers only to the uppermost spectrum. The spectra were recorded at room temperature.

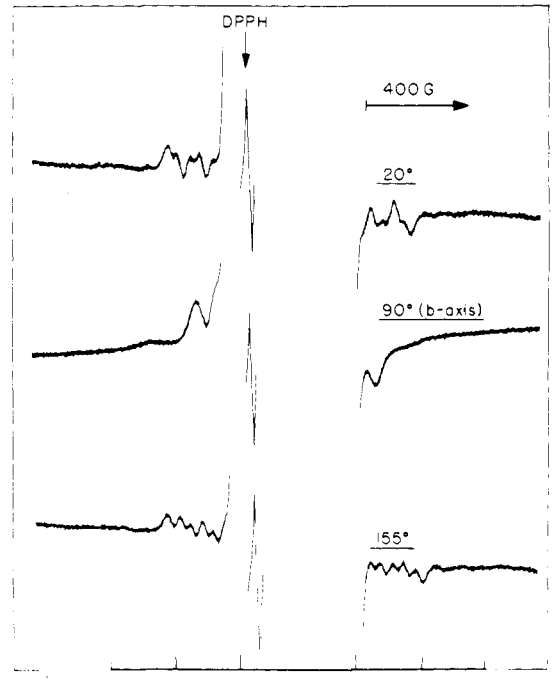

Figure 3. As in Figure 2 but recorded at a tenfold higher gain and wider field sweep. The $|\frac{5}{2}| \leftrightarrow |\frac{3}{2}|$ and $|\frac{3}{2}| \leftrightarrow |\frac{1}{2}|$ fine structure components are brought out while the $\frac{1}{2} \leftrightarrow -\frac{1}{2}$ transitions are well out of scale. The stick diagram refers to the lowest spectrum and denotes the calculated positions of the outermost hyperfine lines for the various fine structure components of one of the Mn^{2+} sites.

Figures 2 and 3 show esr spectra of Mn^{2+},Ca^{2+}-concanavalin A at selected orientations of the magnetic field in the *bc* plane. The strong lines in Figure 2 are associated with the $\frac{1}{2},m \leftrightarrow -\frac{1}{2},m$ transitions. They are approximately 15

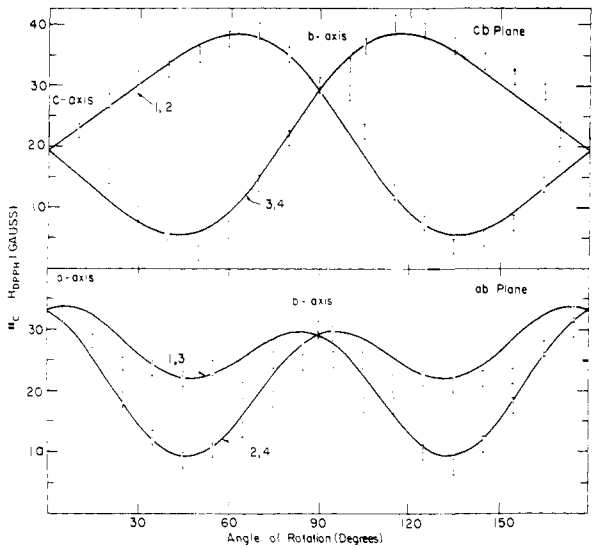

Figure 4. Plots of ΔH *vs.* angle of rotation of the magnetic field in the two crystallographic planes *ab* and *cb*. The curves are calculated from eq 5 with the parameters of Table II. The labeling of the curves corresponds to the numbering of sites in Figure 1.

Gauss (peak to peak) and exhibit a small anisotropy and splitting when the magnetic field is rotated. This anisotropy is a second-order effect which will be discussed in the next section. We also defer to a later section discussion of "forbidden" transitions which appear as weak lines in between the strong transitions. Outside the region of strong lines on both its high and low field sides there are weak, broad bands which are ascribed to the $\pm 5/2 \leftrightarrow \pm 3/2$ and $\pm 3/2 \leftrightarrow \pm 1/2$ fine structure components. The remarkable width of these lines is attributed to a distribution in the ZFS parameters of the protein. They can be seen more clearly in the spectra shown in Figure 3 which were recorded at a higher gain and over a wider range of the magnetic field. They are so broadened as to obscure the hyperfine structure in most orientations, thus preventing quantitative analysis. The spacing between the fine structure components is, however, quite anisotropic and from the maximum separation an order of magnitude of 200–300 G for the ZFS interaction can be estimated. More accurate ZFS parameters can, however, be derived from the small second-order effects of the $M = 1/2$ fine structure transitions.

(ii) Second-Order Anisotropy of the Spectrum. The small anisotropy of the $M = 1/2$ hyperfine lines is not predicted by the first-order approximation but can be accounted for in terms of a second-order correction to eq 2. This gives for the resonance field of the $1/2,m \leftrightarrow -1/2,m$ transitions[20]

$$H(1/2, m) = H_0 + f(D, E, \theta, \phi) - [mA/(g_{Mn}\beta)] - mF \quad (3)$$

where

$$f(D, E, \theta, \phi) = \frac{16}{g_{Mn}\beta H}\{(D - E\cos 2\phi)^2 \times \sin^2\theta\cos^2\theta + E^2\sin^2 2\phi\sin^2\theta - 1/8[D\sin^2\theta + E\cos 2\phi(1 + \cos^2\theta)]^2 - 1/2E^2\cos^2\theta\sin^2 2\phi\} \quad (4)$$

and F includes higher order cross terms between the ZFS and the hyperfine interaction of order $A(\mathrm{ZFS})^2/(g_{Mn}\beta H)^2$. These transitions thus have an anisotropy of the order of $(\mathrm{ZFS})^2/(g_{Mn}\beta H)$. From the symmetry relations discussed above we expect the simplest spectrum when the magnetic field is along a crystallographic axis, since then the spectra of all sites coincide. This spectrum should split into two when the magnetic field is turned away from the axis but remains in a crystallographic plane (see Figure 2).

To obtain the magnitude of the ZFS tensor components and its principal directions relative to the crystallographic axes we performed a best fit analysis of the experimental results of the $1/2 \leftrightarrow -1/2$ transitions in terms of eq 3. In principle all the information could be obtained by analyzing the spectra of a single site in a single plane. To check the model and in order to get more reliable results we analyzed the spectra in the two planes, *ab* and *cb*. The mounting of the crystal in the *ac* plane turned out to be less accurate than in the other two and therefore the data collected in this plane were not included in the final analysis. The analysis of the results was done as follows. To eliminate the m-dependent terms in eq 3 we determined the spacing between the center field of each sextet, H_C, and the reference DPPH signal, H_{DPPH}, and plotted this difference, ΔH, as a function of the orientation of the magnetic field (Figure 4). The uncertainty of the experimental points is represented in the figure as 2 G, although the actual experimental uncertainty varied with orientation and occasionally exceeded this value. From eq 3, ΔH is given by

$$\Delta H = H_C - H_{DPPH} = \delta H + f(D, E, \theta, \phi) \quad (5)$$

where

$$\delta H = H_0 - H_{DPPH} = H_0\frac{g_{DPPH} - g_{Mn}}{g_{DPPH}} = H_0\frac{\Delta g}{g_{DPPH}} \quad (6)$$

For the best fit analysis, the angles θ and ϕ were expressed in terms of the Euler angles α, β, γ of the principal directions of the ZFS tensor and the spherical angles of the magnetic field in the crystallographic coordinate system.[18] The Euler angles and the parameters Δg, D, and E were then taken as free parameters to be determined by best fit to the experimental results. At first, an analysis was made where we assumed axial symmetry ($E = 0$). Although a reasonable, overall fit with the experimental results was obtained, there were systematic deviations of the experimental points which suggested that there was a small but definite contribution from the term E. When this term was subsequently included in the analysis, the fit was indeed considerably improved. The results of the two analyses are summarized in Table II. (The values of g_{Mn} given in this table include a small correction not included in eq 3 of order $A/(g_{Mn}\beta H)$, from second-order effects of the hyperfine interaction.) The continuous curves in Figure 4 were calculated with the parameters of Table II.

Detailed measurements of the hyperfine splitting in the three crystallographic planes show a very slight anisotropy in A ranging between 91.5 and 93.0 G. The smallest value of A was measured when the magnetic field was nearly perpendicular to the major axis of the ZFS tensor. It is therefore likely that the A tensor is axially symmetric or very nearly so, with A parallel to the z axis of the ZFS tensor. With this assumption the following values for the principal components of A are calculated from the experimental results: $A_\parallel = 94.4$ G, $A_\perp = 91.5$ G.

An estimate of the anisotropy of the g tensor depends on the accuracy of the ZFS parameter. The good fit of the experimental points in Figure 4, and the quantitative agreement of the fine structure spectra (Figure 3) and of the relative intensity of the forbidden transitions to be discussed shortly, indicate that these parameters are fairly well established. We estimate the accuracy of the mean value of the major component of the ZFS interaction at ±10 G and, using eq 4, we can then place an uncertainty of ~0.0004 on the g factor, which can also be considered as an upper limit for its anisotropy.

Table II. Magnetic Parameters for Mn^{2+} in Mn^{2+},Ca^{2+}-Concanavalin A

$D/g_{Mn}\beta$, G	$\lambda = E/D$	α, deg	β, deg	γ, deg	g_{Mn}	$A_\parallel/g_{Mn}\beta$, G	$A_\perp/g_{Mn}\beta$, G
232 ± 10	0.185	42 ± 3	54 ± 2	147 ± 3	2.0009 ± 0.0004	94.4	91.5

We have not included in the hamiltonian (eq 1) a quartic zero field splitting term.[21] This interaction does not affect the $M = \frac{1}{2}$ fine structure term in first order and since for Mn^{2+} it seldom exceeds 20 G it should have no effect on the spectrum in our case.

With these results we can now return to the fine structure components with $M \neq \frac{1}{2}$. Although it was not possible to analyze these transitions because of poor resolution, it was possible to identify them from the calculated values of D, E, and the Euler angles. The stick diagram in the lower trace of Figure 3 gives the positions calculated from eq 2 of the outermost hyperfine components in this orientation. It may be seen that these calculated positions indeed correspond to features in the spectra that can be identified with the extreme ends of fine structure bands.

(iii) Forbidden Transitions. In Figure 2 there are weak lines in between the strong lines of the $\frac{1}{2} \leftrightarrow -\frac{1}{2}$ transitions. This is particularly clear in the spectra taken with the magnetic field parallel to a crystallographic axis. These weak lines correspond to transitions of the type $(M,m \leftrightarrow M - 1, m \pm 1)$ and arise from second-order effects associated with cross terms between the ZFS and the hyperfine interaction.[22] For the $M = \frac{1}{2}$ fine structure band, theory predicts that the forbidden lines should appear in pairs, whose sparation depends on g_I of ^{55}Mn, and which are centered on the points midway between the allowed transitions. The experimental spectra are in complete agreement with these expectations and with the known value of g_I. The relative intensity of the forbidden lines compared to the neighboring allowed hyperfine transitions for the $M = \frac{1}{2}$ fine structure band is (for axial symmetry)

$$(D/g_{Mn}\beta H)^2 \sin^2 2\theta\,[64((35/4) - m^2 - m)] \quad (7)$$

The intensities of the forbidden transitions are thus expected to be largest at the center ($m = \pm\frac{1}{2}$). In fact, the calculated intensities (with D from Table II) are in agreement with the experimental spectra. For example, the relative intensity $(\frac{1}{2},\frac{1}{2} \leftrightarrow -\frac{1}{2},-\frac{1}{2})/(\frac{1}{2},\frac{1}{2} \leftrightarrow -\frac{1}{2},\frac{1}{2})$ measured with the magnetic field along the c axis is 0.20 compared to a calculated value of 0.19. The corresponding results for the a axis are 0.09 and 0.17. Similarly the intensity ratio $(\frac{1}{2},\frac{5}{2} \leftrightarrow -\frac{1}{2},\frac{3}{2})/(\frac{1}{2},\frac{5}{2} \leftrightarrow -\frac{1}{2},\frac{5}{2})$ is 0.09 along the c axis as compared to a calculated value of 0.11 (0.06 and 0.10 along the a axis).

Because of the $(ZFS/(g_{Mn}\beta H))^2$ dependence, the relative intensity of the forbidden transitions at X band (ν = 9.2 GHz) is expected to be an order of magnitude greater than at Q band (ν = 35 GHz). In fact, at X band the forbidden transitions are nearly as intense as the allowed transitions, resulting in complicated and poorly resolved spectra.

(iv) Distribution of the ZFS Tensor Parameter. The large width of the $M \neq \frac{1}{2}$ fine structure components may be attributed to distribution in the direction and magnitude of the ZFS components in the single crystal. Such inhomogenous broadening will be largest for lines furthest from the center of the spectrum; for a given site it is largest for the $\pm\frac{5}{2} \leftrightarrow \pm\frac{3}{2}$ fine structure components, half as much for the $\pm\frac{3}{2} \leftrightarrow \pm\frac{1}{2}$ components and to first order does not affect the $\frac{1}{2} \leftrightarrow -\frac{1}{2}$ transitions. The magnitude of the distribution can be related[23] to the average line width, $(\langle \delta h(M,m)\rangle^2)^{1/2}$ by

$$\sqrt{\langle \delta h(M,m)\rangle^2} = [\partial H(M,m)/\partial\theta]\sqrt{\langle \delta\theta\rangle^2} + [\partial H(M,m)/\partial D]\sqrt{\langle \delta D\rangle^2} \quad (8)$$

where $(\langle \delta\theta\rangle^2)^{1/2}$ and $(\langle \delta D\rangle^2)^{1/2}$ are the root-mean-square distributions in θ and D respectively, and we have assumed an axial ZFS tensor. An upper limit can be placed on these quantities by taking the appropriate derivatives of eq 2 and the estimated width of 600–800 G for the $M = \frac{3}{2}$ transition. This gives

$$(\langle \delta\theta\rangle^2)^{1/2} \lesssim 5° \text{ and } (\langle \delta D\rangle^2)^{1/2} \lesssim 80 \text{ G} \quad (9)$$

The distribution in the ZFS parameters also affects the $M = \frac{1}{2}$ transitions, although to a much lesser extent, as their anisotropy is only of second order with respect to the ZFS. In fact it is possible to account for the observed width and its anglar variation in terms of the above results (eq 9), but it must be assumed that there is a significant distribution in both the magnitude and the direction of the ZFS parameters. This follows from the fact that there is an appreciable width even at orientations where either $\partial H/\partial D$ or $\partial H/\partial\theta$ vanish.

Discussion

The results of the present study show that the Mn^{2+} site in the protein has low symmetry, as reflected by the presence of a quadratic ZFS interaction. The magnitude and direction of the ZFS tensor components are not well defined in the crystal and have a rather large distribution, which is much larger than the overall mosaicity of the crystal (estimated by X-ray diffractometry to be less than 1°). This implies that the distribution in the ZFS parameters reflects local disorder in the metal binding site. X-Ray studies show that the metal–ligand distance is about 2.8 Å, considerably larger than the usual manganese–ligand distance in simple complexes (2.0 Å), which leads one to suspect that it is a distribution in the ligand structure around the metal ion which is responsible for the spread in the ZFS parameters.

Our results show that the major axis of the ZFS tensor is inclined at about 50° to the crystallographic axes. These results will be of importance in the refinement of the structure of the concanavalin A transition metal binding site from X-ray measurements.

Acknowledgment. We thank Shimon Vega for helpful discussion and assistance in computation.

References and Notes

(1) J. B. Sumner and S. F. Howell, *J. Bacteriol.*, **32**, 227 (1936).
(2) A. J. Kalb and A. Levitzki, *Biochem. J.*, **109**, 669 (1968).
(3) J. Yariv, A. J. Kalb, and A. Levitzki, *Biochim. Biophys. Acta*, **165**, 303 (1968).
(4) A. J. Kalb and A. Lustig, *Biochim. Biophys. Acta*, **168**, 366 (1968).
(5) J. Greer, H. W. Kaufman, and A. J. Kalb, *J. Mol. Biol.*, **48**, 365 (1970).
(6) J. Weinzierl and A. J. Kalb, *FEBS (Fed. Eur. Biochem. Soc.) Lett.*, **18**, 268 (1971).
(7) G. M. Edelman, B. A. Cunningham, G. N. Reeke, Jr., J. W. Becker, M. J. Waxdal, and J. L. Wang, *Proc. Nat. Acad. Sci. U. S.*, **69**, 2580 (1972).
(8) K. D. Hardman and C. R. Ainsworth, *Biochemistry*, 11, 4910 (1972).
(9) C. Nicolau, A. J. Kalb, and J. Yariv, *Biochim. Biophys. Acta*, **194**, 67 (1969).
(10) G. H. Reed and M. Cohn, *J. Biol. Chem.*, **245**, 662 (1970).
(11) T. Yonetani, H. R. Drott, J. S. Leigh, Jr., G. H. Reed, M. R. Waterman, and T. Asakura, *J. Biol. Chem.*, **245**, 2998 (1970).
(12) G. H. Reed and W. J. Ray, Jr., *Biochemistry*, **10**, 3190 (1971).
(13) J. C. W. Chien and E. W. Westhead, *Biochemistry*, **10**, 3198 (1971).
(14) M. Cohn, J. S. Leigh, Jr., and G. H. Reed, *Cold Spring Harbor Symp. Quant. Biol.*, **36**, 533 (1971).
(15) G. H. Reed and M. Cohn, *J. Biol. Chem.*, **247**, 3073 (1972).
(16) E. Melrovitch, Z. Luz, and A. J. Kalb, *J. Amer. Chem. Soc.*, **96**, 7542 (1974).

(17) A. D. Rae, *J. Chem. Phys.*, **50**, 2672 (1969).
(18) H. Goldstein, "Classical Mechanics," Addison-Wesley, London, 1959, p 109.
(19) A. Abragam and B. Bleaney, "Electron Paramagnetic Resonance of Transition Ions," Clarendon Press, Oxford, 1970, p 205.
(20) W. Low, "Solid State Physics," Suppl. 2, Academic Press, New York, N.Y., 1960, p 57.
(21) Reference 20, p 116.
(22) Reference 19, p 186.
(23) D. Shaltiel and W. Low, *Phys. Rev.*, **124**, 1062 (1961).

Electron Spin Resonance Spectroscopy of Aqueous Solutions of Concanavalin A

Eva Meirovitch, Zeev Luz,* and A. Joseph Kalb (Gilboa)

Contribution from the Isotope Department and the Department of Biophysics, The Weizmann Institute of Science, Rehovot, Israel. *Received March 7, 1974*

Abstract: A detailed analysis of the esr spectra of aqueous solutions of concanavalin A at Q-band frequency is presented. Three species were studied: (i) Mn^{2+}-concanavalin A; (ii) Mn^{2+},Ca^{2+}-concanavalin A, and (iii) the α-methyl glucoside complex of the latter form. The spectra correspond to high spin Mn^{2+} at the slow tumbling limit where only the $-\frac{1}{2} \leftrightarrow \frac{1}{2}$ fine structure transitions are observable. The other transitions are smeared out by the large anisotropy due to the quadratic zero field splitting interaction. The $-\frac{1}{2} \leftrightarrow \frac{1}{2}$ transitions exhibit sufficient structure due to second-order effects to allow a detailed analysis of the magnetic and dynamic parameters. It was found that in all three forms they are identical within the experimental accuracy to those found in single cyrstals of Mn^{2+},Ca^{2+}-concanavalin A. Theoretical spectra of the $-\frac{1}{2} \leftrightarrow \frac{1}{2}$ transitions were calculated for different values of line width and rotational correlation times and compared with the experimental spectra. From the line shape analysis, information on the correlation times associated with the Mn^{2+} ions in the various concanavalin A forms was derived. It was found that for species ii and iii these correlation times could be identified with the diffusion of the molecule. In species i, *i.e.*, Mn^{2+}-concanavalin A, the observed correlation times were shorter, indicating some extra mobility of the Mn^{2+} binding site.

In the preceding paper[1] (henceforth referred to as I) we discussed the esr spectrum of single crystals of Mn^{2+},Ca^{2+}-concanavalin A. We here extend this work to esr studies of concanavalin A solutions. When Mn^{2+} is bound at the transition metal binding site, S1, a characteristic spectrum, is observed. The spectrum changes when Ca^{2+} is bound at the Ca^{2+} binding site, S2. No further changes are observed when α-methyl glucoside is bound to the protein.[2] These spectra have not been understood in enough detail to allow their quantitative interpretation in terms of the structure of the transition metal binding site. The magnetic parameters derived in I have aided us in the analysis of the solution spectra of Mn^{2+}-concanavalin A, Mn^{2+},Ca^{2+}-concanavalin A, and its α-methyl glucoside complex, which we present here. We find that the magnetic parameters of the Mn^{2+} in the various concanavalin A species are practically the same as in the single crystal of Mn^{2+},Ca^{2+}-concanavalin A. However, the measurements yielded new information on the dynamics of the Mn^{2+} site. It is shown that the correlation time for Mn^{2+}-concanavalin A is considerably shorter than for the other two species, in which S2, or S2 and the saccharide binding site are occupied.

The spin hamiltonian of the Mn^{2+} ions in single crystals of Mn^{2+},Ca^{2+}-concanavalin A was determined by studies of the angular dependence of the esr spectrum. If the small anisotropy in the hyperfine tensor and the small asymmetry in the ZFS interaction are neglected, it is found to have the form

$$\mathcal{H} = g_{Mn}\beta HS + ASI + D\left[S_z^2 - \frac{1}{3}S(S+1)\right] \quad (1)$$

As discussed in I, this hamiltonian yields a spectrum consisting of five fine structure bands each split into six hyperfine components. The line shape of the solution spectrum depends on the dynamics of the Mn^{2+} site. In the slow motion limit, which is often the case for protein molecules, the spectrum may approximate that of a powder. Analysis of such spectra in manganese binding proteins has been attempted before.[2,3] For the case $D \ll g\beta H$ one expects only the $-\frac{1}{2} \leftrightarrow \frac{1}{2}$ ($M = \frac{1}{2}$) fine structure components to give strong absorption peaks, corresponding to $\frac{9}{35} = 0.26$ of the total esr intensity. The rest of the transitions, *i.e.*, the $M \neq \frac{1}{2}$ fine structure components, are either very weak or completely smeared out because of their large anisotropy. In the powder, the $M = \frac{1}{2}$ transition has an overall width of the order D^2/H due to second-order anisotropy in the ZFS term. When there is sufficiently rapid rotational motion the line shape is sensitive to the magnitude of the rotational correlation time associated with the Mn^{2+} ion. Thus, the line shape can be used to study the dynamics of the metal binding site of the protein solution.

We have found that, in fact, only the $-\frac{1}{2} \leftrightarrow \frac{1}{2}$ transitions of the Mn^{2+} spectra are observed in concanavalin A solutions. Their line shape is affected strongly by binding of Ca^{2+} but also by changes in pH and temperature. These effects can be accounted for in terms of rotational motion of the Mn^{2+} site, and we have derived correlation times for the various cases. The general theory used to derive the correlation times is reviewed in section II. The analysis of the spectra is given in section III, and the results are discussed in section IV. It appears that these correlation times can be identified with the rotational diffusion of the whole protein molecule for Mn^{2+},Ca^{2+}-concanavalin A and its saccharide complex but that in Mn^{2+}-concanavalin A there is a considerably shorter correlation time reflecting an independent more rapid rotation in the Mn^{2+} site.

I. Experimental Section

Concanavalin A, prepared from Jack bean meal as in I, was purchased from Miles-Yeda (Rehovot). The demetallized protein was prepared by dialysis of acidified protein against twice-distilled water as described.[4] The protein was subsequently dialyzed against